JOURNAL OF CATALYSIS 65, 348–358 (1980)

Bimodal Metal Particle Size Distributions of Pd and Pt on Vitreous Supports from SAXS Data

G. COCCO, L. SCHIFFINI, AND G. STRUKUL

Facoltà di Chimica Industriale, Università di Venezia, D.D. 2137, Venice, Italy

AND

G. CARTURAN

Centro di Chimica Metallorganica del CNR, c/o Istituto di Chimica Industriale, Via Marzolo 9, Padua, Italy

Received August 8, 1979; revised March 10, 1980

A study of metal particle size distribution using small-angle X-ray scattering (SAXS) is reported for low-content Pd and Pt catalysts, prepared by reduction with LiH or H_2 of $M(C_3H_5)_2$ (M = Pd,Pt) treated with vitreous supports holding –OH groups on the surface. In the mathematical treatment of SAXS data, both analytical and numerical methods have been employed and compared. Two different sizes in the aggregation state of the metal have been ascertained in all the examined cases, one of which under 30 Å. A comparison with transmission electron microscopy (TEM) results is also presented. The reliability of SAXS technique is discussed in terms of absolute scattering power.

INTRODUCTION

Within the framework of our investigation on Pd and Pt catalysts on vitreous supports (*1–3*), we reported in a preliminary note that the catalytic activity of some low-content Pd catalysts is strictly related to the particle size of the supported metal, which was determined by small-angle X-ray scattering (SAXS) (*4*).

In determining the metal particle dispersion by SAXS, we assumed as a first approach that the particle size distribution function of the dispersed metal could be approximated by a log–normal function (*5–7*) adjusted to the classical parameters: Guinier radius and Porod radius, expressed as ratios of moments of the chosen distribution function.

The dispersion of the metal was obtained by reactions (1), (2), and (3) (*3*):

$$\text{glass}\vdash\!\text{OH} + M(C_3H_5)_2 \longrightarrow \text{glass}\vdash\!M(C_3H_5) + \text{propene}, \quad (1)$$

$$\text{glass}\vdash\!M(C_3H_5) \xrightarrow{(\text{LiH or } H_2)} \text{metal dispersed on glass}, \quad (2)$$

$$M(C_3H_5)_2 \text{ sorbed on glass} \xrightarrow{(\text{LiH or } H_2)} \text{metal dispersed on glass} \quad (3)$$

(M = Pd, Pt)

which suggested the possible existence of two different metal particle sizes since reactions (2) and (3) should occur with different rates. Also related to this hypothesis, the Guinier plots for some of the samples studied by SAXS as given in (*4*) showed a weak curvature in the region of small angles, away from the linear trend used to compute the Guinier radius.

We have been prompted by these obser-

0021-9517/80/100348-11$02.00/0

vations to analyze these systems more accurately in order to trace the existence of different size fractions in the aggregation state of the metal. Thus, we tried to obtain the whole statistic distribution of the metal particle size of these catalysts using SAXS measurements carried out under higher resolution and making use of a suitable mathematical treatment.

Our SAXS investigations were further supported by comparing SAXS data with results obtained from traditional methods of analysis like transmission electron microscopy (TEM) and wide-angle X-ray line-broadening analysis (WAXS). However, SAXS analysis attains a much more complete description of our systems, since the TEM method only allows the examination of a small volume of the sample, and the application of WAXS analysis become critical below 25–35 Å, even for well-crystallized phases (*8–9*).

The support surface areas were also measured by the Brunauer–Emmett–Teller (BET) method and compared with SAXS data.

EXPERIMENTAL

Support and Catalyst Preparation

The general procedure has been described in previous works (*2, 3, 10*).

A slurry of the powdered supports in pentane was allowed to react with an appropriate amount of $M(C_3H_5)_2$ (M = Pd,Pt) in pentane solution under nitrogen. After 2 hr the reaction mixture was degassed and kept under H_2 for 2 hr. The catalysts so obtained were filtered off and dried, evaporating the solvent at reduced pressure. The samples were stored under vacuum and handled with fluxing argon.

In some cases, before reduction with H_2, the $M(C_3H_5)_2$–support reacting mixture was washed several times with pentane to elute unreacted $M(C_3H_5)_2$ sorbed on the glass surface.

Instrumental Methods, Data Collection, and Processing

Crystallite sizes were determined by WAXS using a Philips automatic X-ray powder diffractometer system equipped with a rotating sample holder, graphite monochromator, and proportional detector. Ni-filtered Cu$K\alpha$ radiation with a pulse-height discriminator was employed. The method is based on both the $K\alpha_1\alpha_2$ doublet correction and on the correction for instrumental broadening, according to the literature (*9*); Scherrer's equation was then applied to the diffraction profile.

TEM microphotographs were registered on a Philips EM-200 instrument.

BET measurements were carried out with a C. Erba Sorptomatic 1800 instrument.

SAXS measurements were carried out with a Kratky vacuum camera. A special Philips Mo target X-ray tube was used at 60 kV. A $K\beta$ filter together with pusle height discrimination and a scintillation detector was employed. Front slits of 40 and 60 μm were used. The achieved angular resolution was about 600 Å in Bragg's space. The "infinite-beam" condition was met. The observed intensity was automatically explored with an electronically programmed step-scanner. To ensure satisfactory statistics each diffraction curve was measured a number of times by fixed counting technique, providing that 10^5 counts per point were accumulated to maintain the counting probable error below 1%.

A Lupolen standard (*11*) was periodically used to control the constancy of the primary beam and to determine the absolute values of the scattered intensities, according to the procedure described in Refs. (*12*) and (*13*) in the framework of a unified theory of absolute intensity measurements in SAXS.

It is well known that the "pore maskant" method (*14, 15*) must be used whenever interferences arise between holes and metal scattering, as happened in our study. We

used *syn*-$Br_2C_2H_4$, because its electron density is very close to that of the vitreous support. The pore maskant absorption was performed in a glass apparatus by condensing an exceeding amount of liquid on degassed samples. The *syn*-$Br_2C_2H_4$ container was directly connected to the sample tube and the liquid was kept frozen during the degassing operation. The procedure of removing surplus liquid was checked by using a thermogravimetric balance and by relating the trends so obtained with X-ray attenuation factors concurrently measured. The powdered catalysts as well as their supports were homogeneously dispersed inside plate-like holders and were always kept below 10°C in order to prevent the escape of maskant before and during the SAXS measurements.

For every sample exposed to X rays the effective amount of maskant retained was determined from the decrease in weight occurring when the content of the sample holders was treated for 12 hr at 250°C in vacuum.

The SAXS intensities of the treated supports were subtracted, as was the matrix effect, from the SAXS intensities of the corresponding catalyst after taking into account the related attenuation factors. The mathematical treatment was performed on the curves so obtained.

SAXS Working Equations

In the higher-angle tail of the diffraction curve the intensity $I(h)$ scattered by a two-phase system is related only to two parameters of the system by the equation (*16, 17*)

$$\lim_{h \to \infty} I(h) = \frac{2\pi I_e(h)(\Delta\rho)^2 S}{h^4}, \qquad (4)$$

where

$\Delta\rho = \rho_1 - \rho_0$ is the electron density difference between the two phases ($\rho = \delta \Sigma Z_i/M$; δ = mass density, Z_i = number of electrons in the ith atom, M = molecular weight),

S = the total surface area separating the phases,

$h = 4\pi\lambda^{-1}\sin\theta$ is the modulus of the diffraction vector, λ is the X-ray wavelength and 2θ is the scattering angle,

$I_e(h)$ = is the intensity scattered by a single electron in the same experimental conditions.

Equation (4) holds if a point collimated primary beam is used, whereas with a line-shaped X-ray primary beam the diffraction intensity varies as h^{-3}, if infinite height slits are employed. Using the instrumental variable m (μm) defined in the direct space as the distance between the primary beam and the diffracted ray on the recording plane, it is possible to evaluate the specific surface, expressed in square meters per gram, by the equation (*18, 19*)

$$S_{sp} = \frac{16\pi^2 \lim_{m \to \infty} m^3 J(m)}{a^2\lambda^4 r_e^2 N_A^2 P_0 (\Delta\rho)^2 p} \cdot 10^{-4}, \qquad (5)$$

where

$J(m)$ is the slit-smeared intensity (n_e^2 cps cm^{-2}; n_e stands for the number of electrons and cps for counts per second),

r_e^2 is the Thomson factor (cm^2),

N_A is Avogadro's number.

P_0 is the energy per centimeter of length of the primary beam weakened by the scattering sample and determined by the calibration sample method (cps cm^{-1}) (*11*).

p is the sample thickness obtained by multiplying the sample concentration (g cm^{-3}) by the sample-holder thickness (cm) (*20*).

a is the distance between the sample and the recording plane (cm).

The volume fraction c of the scattering heterogeneities is available according to the relationship (*19*)

$$\int_0^\infty h^2 I(h)\, dh = 2\pi^2 I_e(h)(\Delta\rho)^2 c(1-c)V, \quad (6)$$

where V is the illuminated volume.

Equation (6), for the slit-smeared intensity, using the previous formalism, becomes

$$\langle(\Delta\rho)^2\rangle = (\Delta\rho)^2 c(1-c) = \frac{2\pi \int_0^\infty mJ(m)\, dm}{r_e^2 N_A^2 \lambda^3 a P_0 p} \cdot \delta. \quad (7)$$

If spherical in shape, the particles responsible for the observed scattered intensity can be characterized by the Porod diameter, D_p, which represents their average linear dimension,

$$D_p = \frac{3\int_0^\infty hJ(h)\, dh}{2(1-c)\lim_{h\to\infty} h^3 J(h)} \quad (8)$$

Equation (5) yields information on the magnitude of the interfacial surface directly from the experimental data, without arbitrary assumptions about the underlying texture of the sample under study, but tells us nothing about the size distribution of the heterogeneities within the system. A more complete picture is available from SAXS if some theoretical and experimental conditions are satisfied. If the form factor of the scattering particle is known or supposed and is characterized by a single size parameter, and if multiple scattering is negligible, in the case of widely and randomly separated particles, the observed intensity can be expressed as the integral over the desired particle size distribution function. For a volume distribution function the following equation can be written (*19*):

$$I(h) \propto (\Delta\rho)^2 \int_0^\infty D_V(R) R^{-3} V^2(R) i_0(hR)\, dR, \quad (9)$$

where

$D_V(R)$ is the volumetric distribution function that states the volume of all particles defined by the size parameter R;

$i_0(hR)$ is the intensity scattered by a single particle with radius R and volume $V(R)$.

A second analytical method, derived from Debye's correlation function (*21*), has been employed to get the particle size volume distribution function. It can be shown that the following equation stands for the slit-smeared intensity (*22–24*):

$$D_V(R) \propto R \int_0^\infty [h^3 J(h) - K] [2J_0(hR) + J_1(hR)(hR - 3/hR)]\, dh, \quad (10)$$

where $K = \lim_{h\to\infty} h^3 J(h)$ and J_0, J_1 are zero- and first-order Bessel functions, respectively.

The distribution curves, calculated with both cited methods, have been obtained with a computer program which has been made available by Vonk (*25*).

RESULTS AND DISCUSSION

SAXS is a powerful tool in structural analysis since it allows us, in principle, to ascertain the underlying texture of relatively large volumes of materials. However, its application in catalysis suffers from some limitations: the mathematical data treatment may affect the results and some a priori assumptions on the metal particle geometry are usually required. Moreover, in the case of metals dispersed on porous supports, the necessity to use the "pore maskant" method and the fact that the data arise from the difference between the metal plus support and the support scatterings may introduce a further source of uncertainty into the final results.

In the present work, with the aim of detecting possible multimodal metal particle size distribution functions, we took particular care of the sources of the above uncertainty in the endeavor to limit their incidence on the reliability of SAXS results.

TABLE 1

Characterization of the Supports

	Surface area		D_v (Å)
	SAXS (m^2/g)	BET (m^2/g)	
Support C_{230}	633	341	21
Treated support C_{230}	46	—	16
Support B_{230}	351	204	36
Treated support B_{230}	19	—	49

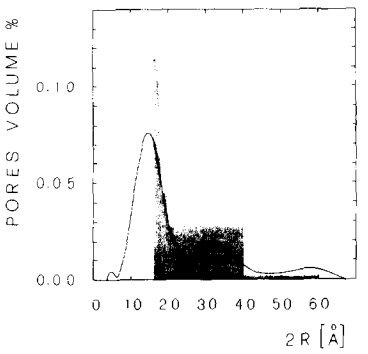

FIG. 1. SAXS and BET pore volume distribution for C_{230}. Shaded area refers to the BET measurements.

All the results discussed here are reported in Tables 1 and 2.

The surface areas of the untreated supports have been obtained by SAXS and BET methods. In Fig. 1, SAXS pore distribution and the corresponding BET histogram of frequency are compared for the C_{230} sample: as can be seen, the histogram shows an edge at 16 Å, since our BET measurements do not take into account pore sizes under this limit. This can explain the differences in the surface areas obtained with the two methods. However, both curves show the same qualitative trend.

The effect of pore maskant in reducing the scattering arising from the micropores of the vitreous supports is shown in Fig. 2, where the SAXS intensity curves of the B_{230} sample before and after treatment with $C_2H_4Br_2$ are compared. Both curves are normalized by the X-ray attenuation factors. The surface areas of the pore maskant treated samples drop from 351 to 19 m^2/g and from 633 to 46 m^2/g, respectively. The presence of these residual surface areas can be ascribed to both occluded and unmasked holes. Actually the volume pore distribution function for treated supports shows a peak in the same position as the main maximum observed in the analogous distributions for the untreated supports. This comparison is emphasized in Fig. 3 for C_{230}, where the distribution functions have been plotted in absolute scale by referring the volume fraction of the holes to the volume obtained from Eq. (7). Consequently this residual scattering has to be subtracted from the catalyst curves in order to obtain the scattering from the metal phase alone.

In spite of the good reproducibility of the amount of pore maskant used both for supports and catalysts (the uncertainty was never found to exceed ±3% out of 12 experiments), a positive linear deviation

TABLE 2

Characterization of the Catalysts

Catalyst	Metal surface area (m^2/g)	D_v (Å)	Metal concentration		Average crystallite size (Å)
			(SAXS) (wt%)	(Elemental analysis) (wt%)	
Pd 0.8 wt% on B_{230}	106	48	0.91	0.85	41
Pd 0.8 wt% washed	191	26	0.26	0.32	—
Pt 1.0 wt% on B_{230}	35	80	0.92	1.00	66
Pt 1.0 wt% washed	49	57	0.30	0.31	58
Pt 1.0 wt% on C_{230}	84	33	0.79	1.00	52
Pt 0.3 wt% on C_{230}	150	19	0.32	0.30	—

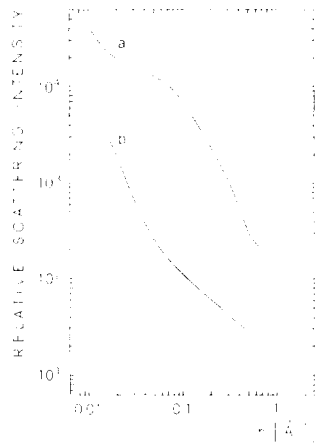

FIG. 2. Effect of *syn*-$C_2H_4Br_2$ on SAXS of C_{230} support: relative scattering intensity for unmasked sample (a) and masked sample (b).

from the Porod law (*16, 17*) in the higher-angle region of our investigation was observed in the catalyst scattering curves, even after subtracting the matrix effect (see Figs. 4 and 5). This fact was ascribed to both the slight difference in the amount of liquid used and the sample background scattering due to the electron density fluctuation within the metal particles (*26*). In this case the subtraction of a constant intensity term allows the computation of the corrected radial intensity for the determination of the SAXS parameters. The opportunity for this correction is validated later on, when the reliability of intensity data is discussed in terms of absolute scattering power.

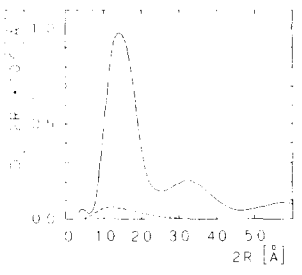

FIG. 3. Characterization of the support C_{230}: pore distribution function of the unmasked (——) and (– – –) masked samples. The curves were obtained by inversion of data of Fig. 2 via Eq. (9) and are plotted as pore volume fraction calculated by Eq. (7).

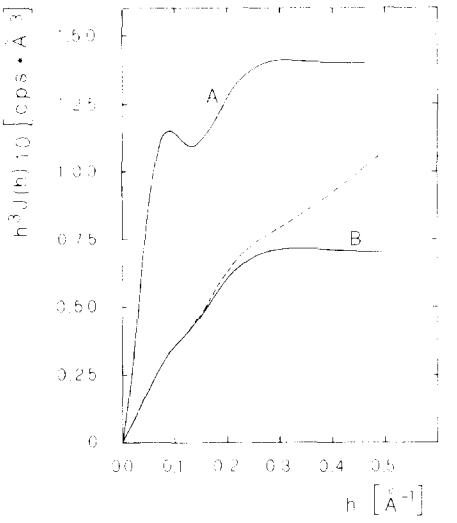

FIG. 4. $h^3J(h)$ vs h functions for Pd 0.85% on B_{230}: (A) nonwashed (0.85% Pd); (B) washed (0.32% Pd). The broken curve refers to the washed sample and represents the experimental trend after subtracting support scattering; when plotted vs h^3 it shows an ascending straight line: its slope is the additional constant intensity subtracted in order to obtain curve (B).

Multiple scattering was found negligible for all the filled samples according to Perret and Ruland (*27*).

Using the two mathematical methods

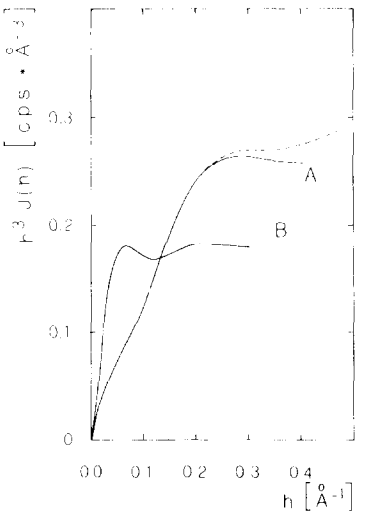

FIG. 5. $h^3J(h)$ vs h functions for (A) Pt 1.0% on C_{230} and (B) Pt 1.0% on B_{230}. Broken curve refers to the former sample and is another example of deviation from Porod the law (see Fig. 4).

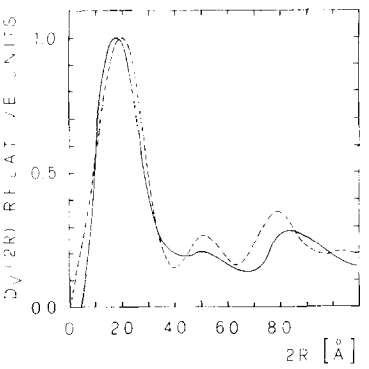

FIG. 6. Metal particle size distribution functions for Pt 1.0% on C_{230}: (——) from Eq. (9); (– – –) from Eq. (10).

specified under Experimental (*19, 25*) the distribution functions of the metal particle size dispersed on the above characterized supports were calculated. Although these two procedures differ greatly in theoretical approach, and despite the different numerical problems involved (for example, the second method—Eq. (10)—is very sensitive to the extrapolated parts of the intensity curve), we have found a satisfactory agreement in the results obtained. For instance, a comparison of the two distribution functions plotted vs the particle diameter in the cases of 1 and 0.3% Pt on C_{230} is shown in Figs. 6 and 7, respectively. This systematic good agreement, verified in all the examined cases, justifies full confidence in the main details of the distribution functions. However, the first method, Eq. (9),

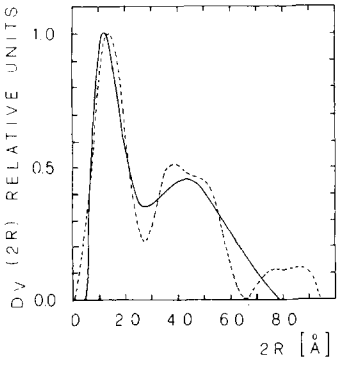

FIG. 7. Metal particle size distribution functions for Pt 0.3% on C_{230}: (——) from Eq. (9); (– – –) from Eq. (10).

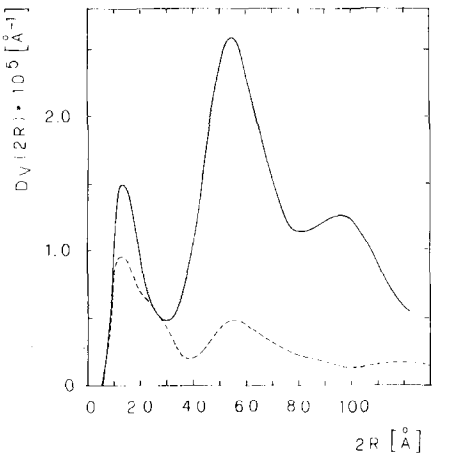

FIG. 8. Metal particle size distribution functions of Pd 0.85% on B_{230}: (——) nonwashed (0.85% Pd); (– – –) washed (0.32% Pd). Quoted also in Ref. (*3*).

has been preferred since it does not require a cumbersome fitting procedure in order to smooth the intensity curves: the distributions reported in this paper refer to that method.

Figure 8 refers to 0.85% Pd on B_{230}, nonwashed and washed before reduction to metal (reactions (2) and (3)).

Figure 9 refers to a similar comparison for 1% Pt on the same support, B_{230}.

As can be seen for all the samples studied, it is possible to locate at least two main peaks in the metal distribution functions, one of which ranges in the <30-Å-diameter interval. The number of metal particles larger than 30 Å is strongly reduced in the

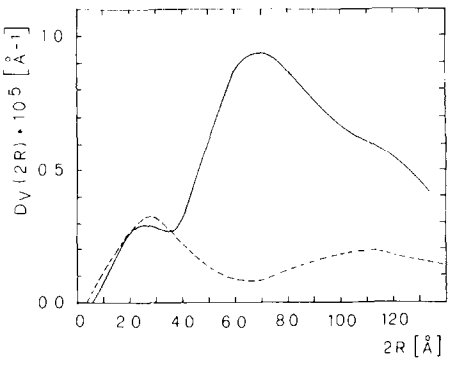

FIG. 9. Metal particle size distribution functions of Pt 1.0 on B_{230}: (——) nonwashed (1.0% Pt); (– – –) washed (0.31Pt).

case of the samples washed before reduction with H_2; whereas, the amount of metal in the <30-Å interval remains practically unchanged. By washing, the sorbed $M(C_3H_5)_2$ complex unreacted with the surface –OH groups (reaction (1)) is partially eluted. Therefore, the results obtained were interpreted by considering the more highly dispersed metal generated from the reduction of the anchored species glass |—$M(C_3H_5)$, while the sorbed $M(C_3H_5)_2$ bears larger metal aggregates (*3*). Moreover, the population of metal particles in the <30-Å interval is in agreement with the extent of reaction (2) as calculated from the amount of propene evolved (*3*). Since the metal particles with dimensions larger than 30 Å give a very small contribution to the catalytic activity in olefin hydrogenation (*1, 4, 28*), the chemical interactions between support and chemical precursor to the metal play a leading role in affecting the catalytic power of these materials.

However, the association of the peak under 30 Å with the metallic phase might be questionable. The systems under investigation are composed of three phases: metal, voids, and support material. The use of pore maskant for both the catalyst and the support, and the subtraction of the relative scatterings, should in principle eliminate the inaccessible pore scattering. Indeed, the possibility of a different number of unmasked holes in the catalyst compared to that of the support, can bias the obtained intensity. As a consequence, a possible systematic artifact might arise in the metal distribution functions in the region of small dimensions.

A first answer to this problem comes from TEM observations which confirm the presence of two ranges in the particle size distribution, in agreement with SAXS determinations. We report, for example, the TEM micrographs relative to 1% Pt on B_{230} (Figs. 10A and B): the fraction of small metal clusters that can be singled out in Fig. 10B, becomes prevalent in the corresponding washed sample (Fig. 11) according to SAXS distributions. From TEM data the assumption of a spheroidal geometry of the metal particles appears justified and it is also confirmed that the pores, as can be seen in Fig. 11 for B_{230} support, have approximately the same size as the small metal particles.

Nevertheless we have tried to attribute the first peak to the metallic phase alone, by using a SAXS self-consistent method.

The "scattering power" for the examined catalysts can be expressed by the equation (*18, 19*)

$$\langle(\Delta\rho)^2\rangle = c_M(\rho_M - \langle\rho\rangle)^2 + c_S(\rho_S - \langle\rho\rangle)^2 + c_P(\rho_P - \langle\rho\rangle)^2, \quad (11)$$

where c_M, c_S, c_P are the volume fractions of metal, support and pores, respectively, with $c_M + c_S + c_P = 1$ and ρ_M, ρ_S, ρ_P are the respective electron densities with average value $\langle\rho\rangle = c_M\rho_M + c_S\rho_S + c_P\rho_P$.

We have compared experimental values of $\langle(\Delta\rho)^2\rangle$ obtained from Eq. (7) to the corresponding theoretical values calculated from Eq. (11) using the metal concentration known from chemical analysis and a variable void volume fraction.

In Fig. 12 the plots of the calculated $\langle(\Delta\rho)^2\rangle$ values vs variable c_P values are reported in the cases of the indicated samples (full lines). We selected these catalysts since the interference of residual unmasked voids, owing to the low metal concentration, may be even more intense. The experimental scattering power data, reported at $c_p = 0$ as marked points, appear to agree with the corresponding theoretical values extrapolated at $c_p = 0$. As shown, the differences between the experimental $\langle(\Delta\rho)^2\rangle$ and the corresponding intercepts are not systematically positive. Thus, a significant contribution to the scattering from the residual unmasked voids can be excluded, differences arising from the complicated handling procedure and from the uncertainties in the elemental analysis.

The calculation of $\langle(\Delta\rho)^2\rangle$ from the experimental data allows the determination of

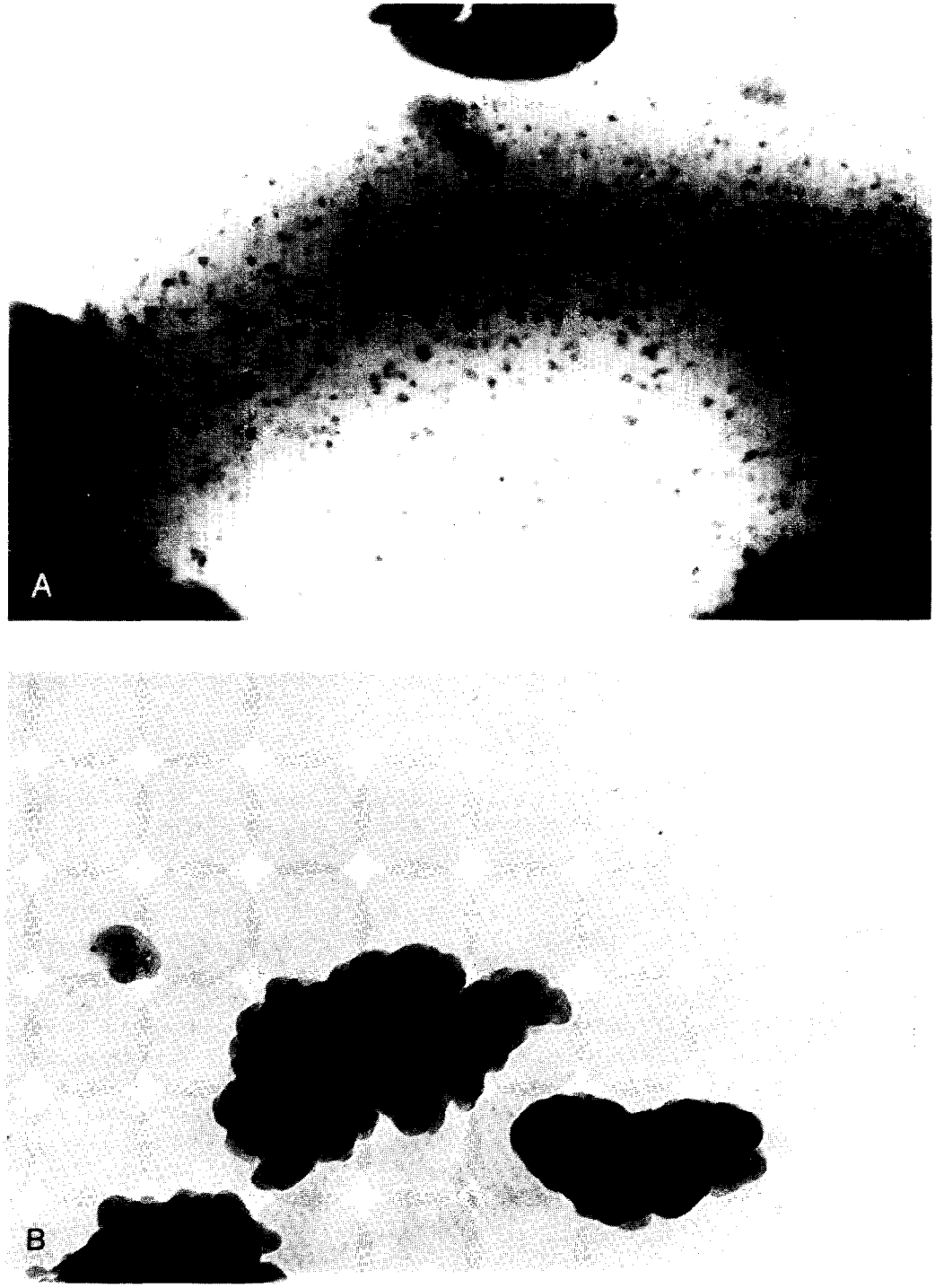

FIG. 10. Transmission electron micrographs of the catalysts Pt 1.0% on B_{230}: (A) ×80,000; (B) ×176,000.

FIG. 11. Transmission electron micrographs of the Pt 1.0% washed sample on B_{230} (effective Pt% = 0.31); ×176,000.

the metal concentrations, which are shown in column 4 of Table 2 transformed to weight percentage.

Surface areas and Porod diameters are also reported.

Average crystallite sizes determined by WAXS analysis, which represent a volume weight mean, are reported for some samples in column 5 of Table 2.

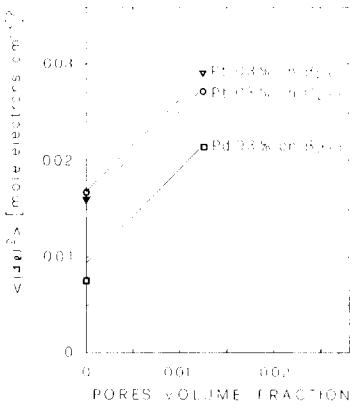

FIG. 12. Comparison between experimental values of "scattering power" (marked points) and calculated values (full lines) in the hypothesis of a three-phase system with an increasing void volume fraction.

In conclusion the physical meaning of the obtained SAXS distribution curves has been explored and the sensitivity of the mathematical treatment has been tested on experimental data. Compared to more traditional techniques SAXS appears as the most versatile method for determining not only the average crystallite size and metal surface area, but also the entire distribution curve.

ACKNOWLEDGMENTS

The authors are grateful to Drs. A. Benedetti and S. Enzo of the Physical–Chemistry Institute of the University of Venezia for help in the experimental work, and to Mr. G. Zenoni of Montedison S.p.A., Porto Marghera, Venezia, for TEM measurements.

We are greatly indebted (particularly L.S) to Professor C. G. Vonk of DMS Central Laboratory, Geleen, Netherlands, for providing the computer program and for valuable suggestions and criticism.

Numerical calculations were performed with a CDC computer, at the Computing Center of Venezia University.

CNR, Roma, is acknowledged for financial support.

REFERENCES

1. Carturan, G., and Gottardi, V., *J. Mol. Catal.* **4,** 349 (1978).
2. Carturan, G., and Strukul, G., *J. Catal.* **57,** 516 (1979).
3. Carturan, G., Cocco, G., Schiffini, L., and Strukul, G., *J. Catal.* **65,** 359 (1980).
4. Cocco, G., Fagherazzi, G., Carturan, G., and Gottardi, V., *J. Chem. Soc. Chem. Commun.* **22,** 979 (1978).
5. Baur, R., and Gerold, V., *Acta Met.* **12,** 1448 (1964).
6. Harkness, S. D., Gould, R. W., and Hren, J. J., *Phil. Mag.* **19,** 115 (1969).
7. Cocco, G., Enzo, S., Fagherazzi, G., Schiffini, L., Bassi, I. W., Vlaic, G., Galvagno, S., and Parravano, G., *J. Phys. Chem.* **83,** 2527 (1979).
8. Adams, C. R., Benesi, H. A., Curtis, R. M., and Meisenheimer, R. G., *J. Catal.* **1,** 336 (1962).
9. Klug, H. P., and Alexander, L E., "X-Ray Diffraction Procedure for Polycrystalline and Amorphous Materials." Wiley, New York, 1974.
10. Carturan, G., Gottardi, V., and Graziani, M., *J. Non-Cryst. Solids* **29,** 41 (1978).
11. Kratky, O., Pilz, I., and Schmitz, P. J., *J. Colloid. Interface Sci.* **21,** 24 (1966).
12. Hendricks, R. W., *J. Appl. Cryst.* **5,** 315 (1972).
13. Shaffer, L. B., and Hendricks, R. W., *J. Appl. Cryst.* **7,** 159 (1974).
14. Gunn, E. L., *J. Phys. Chem.* **62,** 928 (1958).
15. Whyte, T. E., Kirklin, P. W., Gould, R. W., and Heinemann, H., *J. Catal.* **25,** 407 (1972).
16. Porod, G., *Kolloid. Z.* **124,** 83 (1951).
17. Porod, G., *Kolloid. Z.* **125,** 109, 51 (1952).
18. Kratky, O., "Proceeding of the Interdisciplinary Conference on Electromagnetic Scattering." Pergamon, Oxford, 1963).
19. Guinier, A., and Fournet, G., "Small Angle X-ray Scattering." Wiley, New York, 1955.
20. Pilz, I., Glatter, O., and Kratky, O., *Methods in Enzymol.* **61,** 148 (1979).
21. Debye, P., and Bueche, A. M., *J. Appl. Phys.* **20,** 518 (1949).
22. Soulè, J. L., *J. Phys. Radium* **18,** 90A (1957).
23. Donati, J. R., Pascal, B., and Renouprez, A. J., *Bull. Soc. Fr. Mineral Cristallogr.* **90,** 452 (1967).
24. Méring, J., and Tchoubar, D., *J. Appl. Cryst.* **1,** 153 (1968).
25. Vonk, C. G., *J. Appl. Cryst.* **9,** 433 (1976).
26. Ruland, W., *J. Appl. Cryst.* **4,** 70 (1972); Luzzati, V., Witz, J., and Nicolaieff, A., *J. Mol. Biol.* **3,** 367 (1961).
27. Perret, R., Ruland, W., *J. Appl. Cryst.* **4,** 444 (1971).
28. Renouprez, A., Hoang-Van, C., and Compagnon, P. A., *J. Catal.* **34,** 411 (1974).